Journal of Power Sources 195 (2010) 7781–7786

Contents lists available at ScienceDirect

Journal of Power Sources

journal homepage: www.elsevier.com/locate/jpowsour

Short communication

Proton conductivity of ordered mesoporous materials containing aluminium

Monir Sharifi*, Roland Marschall, Martin Wilkening, Michael Wark

Institute of Physical Chemistry and Electrochemistry, Leibniz Universität Hannover, Callinstr. 3A, 30167 Hannover, Germany

ARTICLE INFO

Article history:
Received 12 June 2009
Received in revised form 13 July 2009
Accepted 30 July 2009
Available online 12 August 2009

Keywords:
Proton conductivity
PEMFC membrane additives
Al-MCM-41
^{27}Al MAS NMR
Solid proton conductors
Fuel cells

ABSTRACT

In order to check the influence of Brønsted acidic Al sites in the walls of mesoporous materials on their proton conductivity, we introduced aluminium into the mesoporous SiO_2 framework Si-MCM-41, which possesses hexagonally ordered channels, by using different Al sources, i.e. sodium aluminate, aluminium sulphate and aluminium isopropoxide. The successful synthesis of ordered mesoporous material with incorporated Al species was proven by X-ray diffraction, energy-dispersive X-ray spectroscopy, nitrogen adsorption, scanning electron microscopy and solid state ^{27}Al MAS NMR. By realizing Si/Al ratios of 8–40 it was found that the proton conductivity of the mesoporous aluminium silicates measured by impedance spectroscopy significantly increases with the Al content, reaching a conductivity of 3×10^{-3} S cm^{-1} at 140 °C. The increase of the proton conductivities compared to Al-free Si-MCM-41 results from (i) an improved hydrophilicity enhancing the water storage capability, (ii) a decreased particle size from the micrometer to the nanometer scale (50–100 nm) and (iii) the existing Brønsted acidity in the mesoporous Al-MCM-41. The Al source $NaAlO_2$ gives clearly the best results because the entire Al incorporated within the framework is tetragonally coordinated, while for samples prepared with $Al_2(SO_4)_3$ or AlP also octahedral coordination of oxygen around the Al centers is observed by ^{27}Al MAS NMR.

1. Introduction

Nowadays, an economical and sustainable handling of energy sources, and simultaneously avoiding of any environmental harm, becomes more and more important. In this field, fuel cells are increasingly playing an important role in a hydrogen-based energy economy [1–3]. Functionalized ordered mesoporous silica materials, especially Si-MCM-41, have been found to be attractive additives for the construction of high temperature polymer electrolyte membrane fuel cell (HT-PEMFC) membranes [4,5]. Due to their high hydrophilicity and capillary condensation effects in the narrow channels they can store water and release it again at elevated temperatures, enabling water-assisted proton transport even at temperatures above 100 °C. Enhanced working temperatures of about 140–180 °C, however, are favorable as the cooling of the fuel cell system is simplified, the tolerance towards CO, which poisons the necessary Pt electrocatalyst, is increased, and finally cathode kinetics is faster leading to smaller amounts of the noble metal catalysts required [6]. All these will result in more efficient fuel cell arrangement and higher power densities. Presently, the most used polymer membrane in PEM fuel cell membranes is Nafion® (DuPont), consisting of a perfluorinated backbone with hydrophilic side chains carrying very strong acidic sulphonic acid end groups ($-SO_3H$). The operation temperature of Nafion® is limited to about 80 °C due to the difficulties to maintain a defined high relative humidity which is necessary to avoid the decrease of proton conductivity at higher temperatures [7].

Our approach is to incorporate hydrophilic and preferably water storing particles with intrinsic proton conductivity into the membrane. Recently, we have shown that Si-MCM-41 functionalized with acidic sulphonic acid groups (SO_3H) exhibits, depending on the synthesis route, i.e., grafting or co-condensation, very high proton conductivities [4,5]. We have also demonstrated that, if incorporated into a polymer matrix, with functionalized polysiloxanes or polyoxadiazoles, these functionalized particles improve the proton conductivity of the resulting composite polymer electrolyte membrane (PEM) at high temperatures (180 °C) and low humidity compared to a pure polymer membrane by up to two orders of magnitude [8]. In order to guarantee a good homogenisation and to provide additional mechanical stability, the use of particles with mean diameters in the nm-range is indispensable. Besides of SO_3H-functionalized Si-MCM-41, some zeolites, e.g., mordenite, were also shown to increase the proton conductivity at elevated temperatures if integrated in Nafion®-based hybrid membranes [9]. Detailed impedance and NMR spectroscopy studies have shown that the proton conductivity of ZSM-5 zeolites increases with a decreasing Si/Al ratio of the zeolite because the Brønsted and Lewis acidic centers at the Al sites in the framework support the proton transfer [10–12]. It is, however, problematic to produce large quantities of nm-sized zeolites and, more impor-

* Corresponding author. Tel.: +49 511 762 2943.
E-mail address: monir.sharifi@pci.uni-hannover.de (M. Sharifi).

0378-7753/$ – see front matter © 2009 Elsevier B.V. All rights reserved.
doi:10.1016/j.jpowsour.2009.07.058

tant, their crystal structure is known to be damaged under acidic conditions.

Thus, our actual strategy is to combine the positive effects of mesoporous oxides and zeolites by studying mesoporous aluminium silicates with Al centers in the amorphous walls, but more stable porosity. Therefore, we prepared aluminium containing Si-MCM-41 (in the following named Al-MCM-41) by using different Al sources, i.e., sodium aluminate ($NaAlO_2$), aluminium sulphate ($Al_2(SO_4)_3$) and aluminium isopropoxide (AIP). Apart from the different Al sources the Si/Al ratio was also varied to obtain Al-MCM-41 with a maximum content of Al without destroying the mesoporous character of the material since both factors are important for high proton conductivity and further applications. Characterisation of the synthesized materials was performed using X-ray diffraction (XRD), energy-dispersive X-ray spectroscopy (EDXS), nitrogen adsorption, scanning electron microscopy (SEM) and ^{27}Al magic angle spinning (MAS) nuclear magnetic resonance (NMR) spectroscopy. Proton conductivity values were determined by impedance spectroscopy (IS).

2. Experimental

2.1. Synthesis of Al-MCM-41

Aluminium containing mesoporous Si-MCM-41 was synthesized via three routes mainly differing in the aluminium source used. The synthesized samples were designated as *x*-MCM-41(*y*) where *x* indicates the Al source and *y* the Si/Al ratio. For all syntheses hexadecyltrimethylammoniumbromide (CTAB) was used as surfactant. In the following, synthesis descriptions for *x*-MCM-41(15) are given.

AIP-MCM-41(15) was prepared based on a recipe published elsewhere [13], with some alterations regarding the synthesis temperature which was set to 30 °C and the aging time changed to 4 days. Tetraethylorthosilicate (TEOS) and aluminium isopropoxide (AIP) were used as silica and aluminium sources, respectively. An appropriate amount of 10 mL TEOS was mixed to a 3.7% solution of 0.613 g AIP in 3.83 mL propan-2-ol (PrOH) prepared in an ultrasonic bath. In a second beaker 2.42 g CTAB were dissolved in 120 mL deionized water and 10 mL aqueous ammonia (25 wt.%) at 30 °C. The TEOS/AIP solution was dropped slowly over a period of 15 min to the surfactant/ammonia solution. The molar composition of the final mixture was 1 TEOS:(1/15) AIP:0.147 CTAB:3.04 NH_3:160 H_2O:*z* PrOH. In this route the Si/Al ratio was varied between 15 and 40.

$NaAlO_2$-MCM-41(15) was synthesized by first dissolving 15 g CTAB in 95 mL H_2O at 30 °C [14]. Afterwards an appropriate amount of sodium aluminate (0.626 g) was added under stirring for 2 h. After a clear solution was obtained, 10.65 g sodium silicate was added under stirring immediately followed by sulphuric acid (5.6 g, 10%). The entire solution was then stirred for 30 min before the pH is adjusted to 10 with sulphuric acid (50%). The molar ratio of the individual components of the reaction mixture was 1 Na_2SiO_3:(1/15) $NaAlO_2$:0.4 CTAB:68 H_2O. Following this route samples with Si/Al ratios of 5–40 were synthesized.

For $Al_2(SO_4)_3$-MCM-41(15) first 2.42 g CTAB were dissolved in 120 mL deionized water at 33 °C, then 20 mL aqueous ammonia (25 wt%) were added [13]. Distinct volumes of 10 mL of a 0.146 mol L^{-1} aqueous solution of aluminium sulphate were added. Finally, 10 mL of TEOS were added under stirring to the mixture. The molar composition of the mixture was 1 TEOS:(1/30) $Al_2(SO_3)_4$:0.147 CTAB:6.08 NH_3:160 H_2O. In general, samples with Si/Al ratios between 10 and 40 were prepared by this route.

In all cases the mixtures were transferred to Teflon®-lined autoclaves and heated for 4 days at 100 °C. The synthesis products were recovered by filtration and washed with ethanol and distilled water ($Al_2(SO_4)_3$, AIP). Samples synthesized with $NaAlO_2$ as Al source were washed with 0.1 M H_2SO_4 for ca. 30 min in order to remove all the sodium ions. Afterwards the resulting white solid was dried for 24 h at 100 °C and calcined at 540 °C (heating rate: 1 °C min^{-1}).

2.2. Characterisation

XRD measurements were carried out on a Philips X'Pert diffractometer at room temperature using Cu Kα radiation (λ = 1.5406 Å), with a step size of 0.02° and 5 s measuring time per step. Nitrogen adsorption isotherms at −196 °C were determined on a Quantachrome Autosorb 3B apparatus. Prior to each adsorption measurement, the samples were outgassed at 200 °C for 24 h. The Brunauer–Emmet–Teller (BET) method was used to determine the specific surface area. The pore diameters were calculated according to the Barrett–Joyner–Halenda (BJH) method [15]. SEM and EDXS were determined on a field-emission scanning electron microscope JEOL JSM-6700F with an EDX spectrometer Oxford Instruments INCA 300. In order to obtain representative description of the Si/Al ratio, EDXS measurements were investigated at low magnification in an area of typically 850 μm × 600 μm in order to determine the Si/Al ratios of the washed and calcined samples and especially to check that the samples are sodium free. For the EDXS measurements the samples were pressed into pellets in order to obtain a smooth surface and to minimize the error range of the instrument. Solid state ^{27}Al MAS NMR spectra at a spinning speed of 12 kHz were recorded with an MSL 400 spectrometer (Bruker) which is connected to a shimmed Oxford cryomagnet of a nominal field of 9.4 T. This external magnetic field corresponds to a ^{27}Al resonance frequency of 104.24 MHz. A standard MAS NMR probe (Bruker) was used in combination with rotors of ZrO_2 (4 mm in diameter). Free induction decays (FID) were recorded with a single pulse sequence at room temperature. The 90° pulse length was about 2 μs and the recycle delay was set to 2 s. Up to 2000 FIDs were accumulated for each NMR spectrum. The ^{27}Al MAS NMR spectra were referenced to $[Al(H_2O)_6]^{3+}$ using an aqueous solution of aluminium nitrate.

IS measurements were performed on a Zahner electrochemical workstation IM6e in a frequency range from 1 to 10^6 Hz with an oscillating voltage of 100 mV. The powder samples were prepared as described elsewhere [16]. For the measurements the pellets were placed between two thin graphite slices and then put into a holder made of Teflon® where the pellet is clamped between two sintered metal electrodes. This holder was finally put in the temperature cell of the impedance spectrometer. The relative humidity (RH) can be adjusted using a connected water tank which is individually heatable.

3. Results and discussion

3.1. Characterisation of mesoporous aluminium silicates

The Si/Al ratios of the washed and calcined materials were determined by EDXS and are presented in Table 1. The EDXS results demonstrated that in case of samples prepared with $NaAlO_2$ ion exchange with H^+ ions [17] was successful and led to the complete absence of Na^+ ions in the final products. For the samples prepared with $Al_2(SO_4)_3$ and AIP, as well as for the $NaAlO_2$ samples before washing with H_2SO_4, the Si/Al ratios determined by EDXS are in very good agreement with the desired Si/Al ratios. Thus entire Al provided in the synthesis mixture is incorporated in the framework during synthesis. During washing with H_2SO_4, however, some Al is removed from the framework—the Si/Al ratios discussed in the following are always those of the final products.

Table 1
Lattice constants a_0, surface areas A_s, pore volumes V_p, pore diameters D_p and wall thicknesses T_w for $NaAlO_2$-MCM-41 samples with different Al content, i.e. Si/Al ratio in the walls.

Sample	Si/Al by EDXS	a_0/nm	A_s/m^2 g^{-1}	V_p/cm^3 g^{-1}	D_p/nm	T_w/nm
Si-MCM-41	–	4.531	1031	0.956	2.70	2.027
$Al_2(SO_4)$-MCM-41(20)	19	4.381	854	0.892	2.65	1.731
AlP-MCM-41(20)	22	4.334	830	0.792	2.60	1.734
$NaAlO_2$-MCM-41(20)	21	4.424	1231	1.185	2.68	1.754
$NaAlO_2$-MCM-41(15)	14	4.416	954	0.899	2.64	1.766
$NaAlO_2$-MCM-41(10)	10	4.278	832	0.780	2.41	1.888
$NaAlO_2$-MCM-41(08)	08	4.194	785	0.713	2.28	1.914
$NaAlO_2$-MCM-41(05)	05	–	344	0.285	2.17	–

Powder XRD patterns of hexagonal mesoporous Si-MCM-41 exhibit four characteristic reflections which are indexed as (1 0 0), (1 1 0), (2 0 0) and (2 1 0) [18]. Fig. 1 shows the XRD patterns of the calcined pure silica based and aluminium containing Si-MCM-41 samples with a ratio of Si/Al ≈ 20, respectively. The sharp first (1 0 0) Bragg reflections obtained at $2\theta = 2.11–2.31^\circ$ proof the existence of structured mesopores consisting of channel-type pores with diameters of about 2–3 nm [19,20]. In addition, two weaker peaks ascribed to the (1 1 0) and (2 0 0) reflections were found indicating the typical hexagonal order of the channel pores in the obtained materials. Although the intensity of these reflections is lower for the Al-MCM-41 compared to the pure Si-MCM-41, their existence demonstrates that the long-range hexagonal ordered structure is still maintained after incorporation of aluminium in the framework. Furthermore, XRD patterns recorded at higher angles up to 80° showed no peaks. Therefore, the presence of any crystalline aluminium containing species can be excluded. In general, compared to pristine Si-MCM-41, aluminium containing Al-MCM-41 samples possess a less ordered mesoporous structure indicated by the decreased intensity of all reflections (Fig. 1). However, intensity deterioration and broadening of the XRD reflections is a typical behaviour for Al-MCM-41 [20], because the incorporation of Al into the walls alters their electron density, and at the same time the electron density contrast to the empty pores which is responsible for the appearance of all the peaks. The more pronounced are the shift in the peak positions to higher angles the higher the Al content. This indicates a decrease in the lattice constants which in principle can be the result of reduced channel pore diameters or thinner pore walls.

The pore diameters as well as the inner surface areas and the pore volumes can be determined by adsorption–desorption measurements using nitrogen (N_2) as probe gas, performed of the calcined materials. The isotherms obtained for the calcined Al-MCM-41 samples are shown in Fig. 2; the values for the inner surface area (estimated according to the BET formalism), the pore volumes, the pore diameters deduced from the isotherms are listed in Table 1 and are in fair agreement with literature data [21]. By subtracting the pore diameters from the lattice constants a_0, determined from the positions of the (1 0 0) reflections in the XRD patterns, also the thickness of the walls is obtained. The nitrogen adsorption–desorption isotherms exhibit a shape typical for type IV isotherms [22] and confirm the characteristic features for the presence of mesopores with diameters in the range of 2–3 nm for all samples. At low relative pressures the adsorbed amount increases continuously due to monolayer adsorption followed by multilayer adsorption. A strong increase in the adsorbed amount occurs at relative pressures of 0.2–0.4 due to capillary condensation of nitrogen in the mesoporous channels. The sudden increase in the adsorption ($p/p_0 > 0.9$) and narrow hysteresis loop for the sample $NaAlO_2$-MCM-41(20) at high relative pressures ($p/p_0 > 0.5$) are caused by the condensation of nitrogen in the interstitial space between particles (void spaces) and cracks inside the $NaAlO_2$-MCM-41(20) particles [5,22]. The pore diameters were calculated from the isotherms by using the Barrett, Joyner and Halenda (BJH) method [15] and are plotted in the inset of Fig. 2. For samples with a Si/Al ratio of 20 they lie in the range of 2.4–2.7 nm, the latter value being almost equal to that of Al-free pure Si-MCM-41. With increasing Al content in the samples, however, the pore diameters shrink continuously. For example, for the series of $NaAlO_2$-MCM-41 made with $NaAlO_2$, showing for a Si/Al ratio of 20 the diameter is 2.68 nm but finally reaches 2.28 nm for a Si/Al ratio of 8 (Table 1). The decrease in

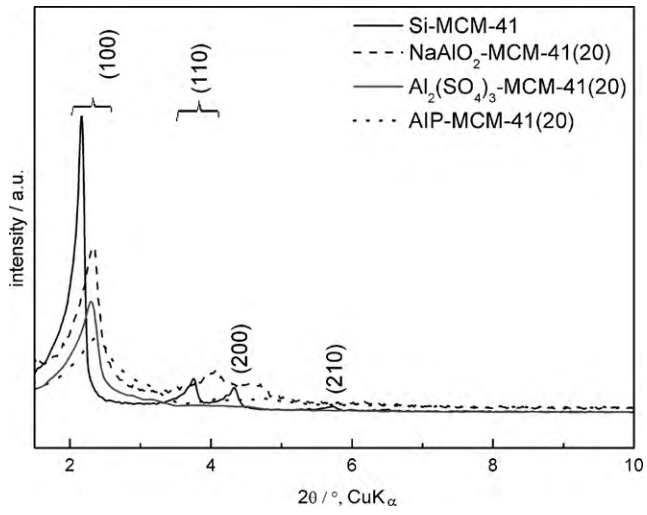

Fig. 1. X-ray diffraction patterns of Si-MCM-41 and Al-MCM-41(20) samples synthesized with different Al sources.

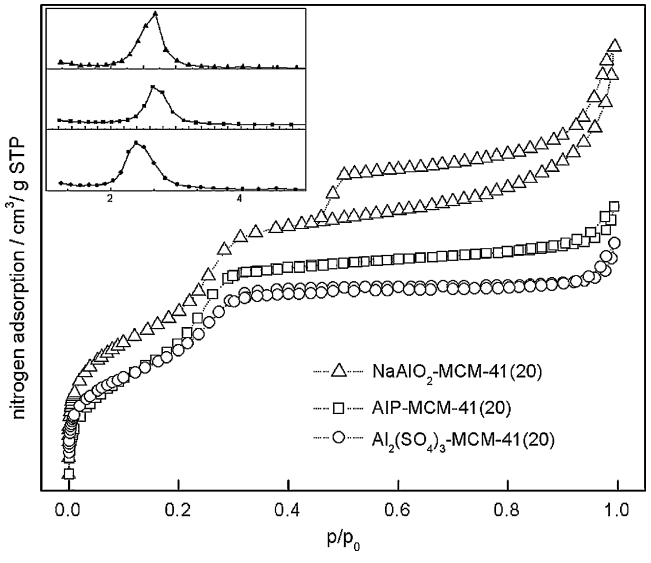

Fig. 2. Nitrogen adsorption–desorption isotherms and pore diameters of Al-MCM-41(20) samples synthesized with different Al sources.

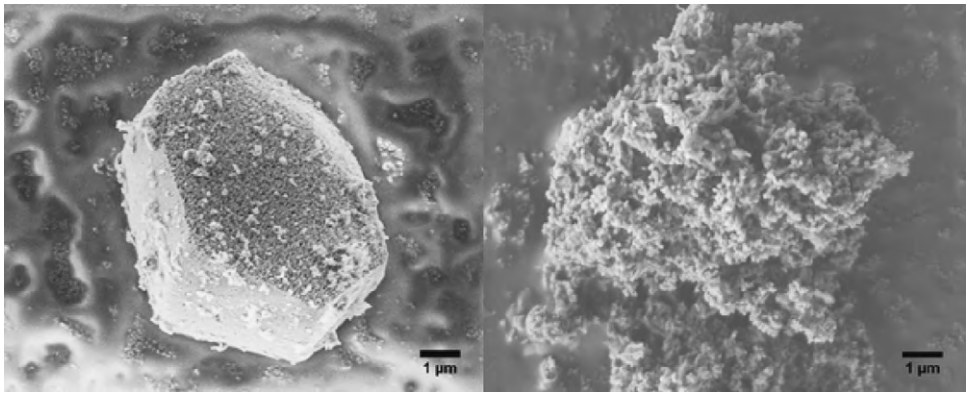

Fig. 3. SEM pictures of Si-MCM-41 (left) and $NaAlO_2$-MCM-41(20) (right).

pore diameter goes in line with the decrease in lattice constants indicating that the pore wall thicknesses remain almost constant.

As seen in the scanning electron micrographs of Fig. 3 the incorporation of aluminium into the silica-framework of Si-MCM-41 changes the size and morphology of the particles from typically 4 to 5 μm to the nm-range. This change is ascribed to the addition of aluminium since apart from that, the synthesis routes of Si-MCM-41 and Al-MCM-41 materials are nearly identical. The $NaAlO_2$-MCM-41 samples consist of nanoparticles with a narrow grain size distribution and grain sizes of 100–120 nm [23]. The nanograins agglomerate easily but they can be separated again by treatment in an ultrasonic bath for 30 min.

3.2. Proton conductivity

The proton conductivities of the different Al-containing *x*-MCM-41(20) samples compared to Al-free silica based Si-MCM-41 are shown in Fig. 4. As a result of the incorporation of aluminium into the walls, the proton conductivity is obviously increased compared to Si-MCM-41 for all samples in the entire temperature range. $NaAlO_2$-MCM-41 shows the best results among these, exhibiting two orders of magnitude higher proton conductivity than observed for pure Si-MCM-41, resulting in a value of 10^{-4} S cm^{-1} at 140 °C. The main reason for the enhanced proton conductivity is the creation of Brønsted acid sites [13,20].

Similar to modified Si-MCM-41, in which organic linkers with proton accepting or donating SO_3H, SO_3^- [4,5] or imidazole [16] head groups were anchored to the inner pore wall surface, the Brønsted acid sites act as places for proton docking on the inner surface of the mesoporous Al-MCM-41 material. Analogous to the situation in zeolites, where protons or other cations are also weakly coordinated to the Al centers in the framework but are nevertheless mobile if suitable solvents are present, leading to fast ion exchange rates or high activity in acidic catalysis [24,25], a high number of Brønsted sites increases the concentration of mobile protons. Furthermore, the distances between the Brønsted sites decreases, which also supports the proton hopping because the hopping probability is distance dependent [8a]. Thus, the proton conductivity increases compared to the pristine Si-MCM-41.

Additionally, the hydrophilic behaviour of the Al-MCM-41 is enhanced compared to that of pure mesoporous Si-MCM-41 as found in water adsorption measurements (Fig. 5). The run of the adsorption curves is again typical for mesoporous materials showing a strong increase in water uptake resulting from capillary condensation in the pores at $p/p_0 \approx 0.5$. The enhanced water adsorption capacity especially of sample $NaAlO_2$-MCM-41(20) and the higher storage probability for water are caused by the increased hydrophilic character of the walls of the mesopores due to the presence of Brønsted acid sites (see Fig. 6). Again $NaAlO_2$-MCM-41 shows the best results for the materials synthesized with different Al sources at Si/Al = 20, incorporating water as much as 80 wt.% of its dry weight. The improved adsorption abilities are very important for the proton conductivity as water molecules strongly support the proton transport [26,27]. We also found that as long as the meso-

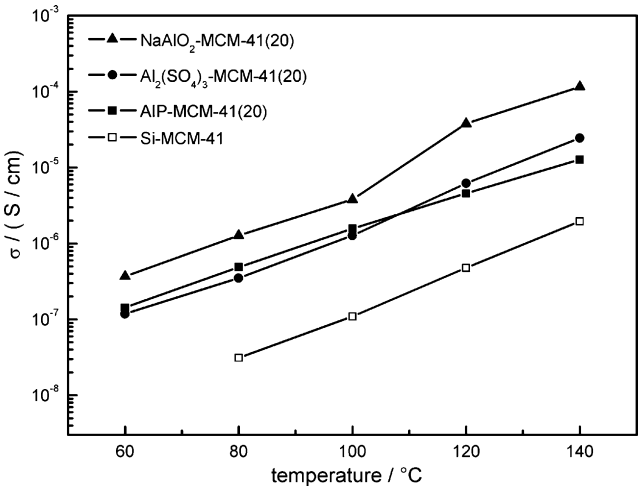

Fig. 4. Proton conductivities for Al-MCM-41(20) at 100% RH compared to pristine Si-MCM-41. The lines are only to guide the eyes and have no physical meaning.

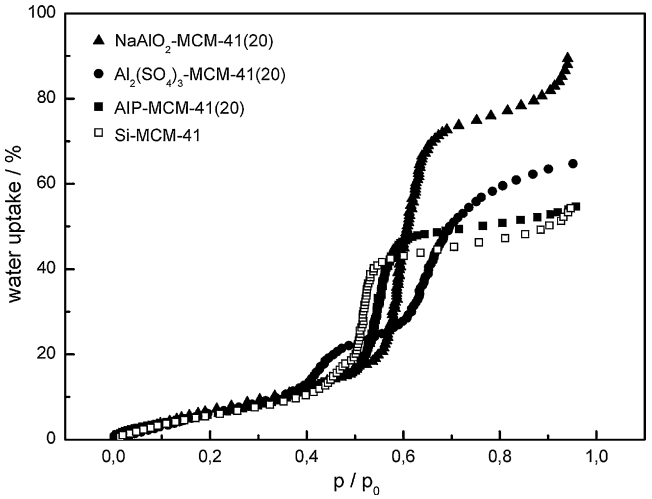

Fig. 5. Water adsorption isotherms for Al-MCM-41(20) samples synthesized with different Al sources compared to pristine Si-MCM-41.

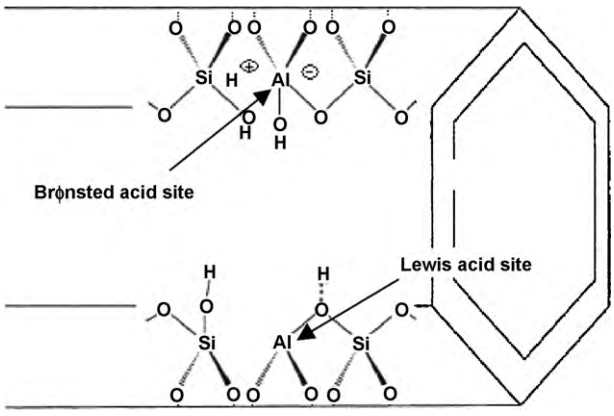

Fig. 6. Internal pore surface of Al-MCM-41.

porous structure is intact, the amount of adsorbed water is higher the more aluminium is incorporated in the framework.

Besides the Brønsted acid sites and increased water adsorption capacity, the reduced particle size (see Fig. 3) is also responsible for the improved proton conductivity of aluminium containing Si-MCM-41 materials, because possible inhomogeneties in the Brønsted sites distribution deep in the interior of the channels become less important. The increased external surface of the nanoparticles will also support the proton transfer. However, in an earlier work comparing SO_3H-functionalized Si-MCM-41 nanoparticles with dense SO_3H-functionalized Aerosil particles of a 10 times smaller size, an observed higher proton conductivity for the SO_3H-functionalized Si-MCM-41 samples demonstrated that proton transfer along the straight internal channel surface is more effective than along the external particle surface [28].

Among the Al-MCM-41 samples with a Si/Al ratio of 20 $NaAlO_2$-MCM-41(20) exhibits higher proton conductivities than $Al_2(SO_4)_3$-MCM-41(20) and AIP-MCM-41(20) which both show almost similar performance in the IS measurements. The ^{27}Al MAS NMR spectra of the samples explain this behaviour (Fig. 7). The NMR spectrum of $NaAlO_2$-MCM-41(20) shows only a single resonance at around 55 ppm [13,20] which is ascribed to tetrahedrally coordinated aluminium. This coordination is only found if aluminium, identical to the situation in zeolites, is perfectly integrated into the aluminium silicate network constructing the walls. For thermodynamical reasons Al in aluminium oxide species possibly deposited in the pores or Al in dangling sites will prefer octahedral oxygen coordination only [13]. In the NMR spectra of the samples prepared from aluminium isopropoxide or aluminium sulphate, exactly such octahedrally coordinated Al species show up leading to NMR lines at around 0 ppm. Although these are less intense than the dominant resonances at around 55 ppm, the two ^{27}Al NMR spectra indicate that a significant fraction of Al is deposited somewhere in the pores. However, only tetrahedrally coordinated Al creates Brønsted acid sites and thus this part of Al cannot contribute to the proton transport [29]. It is evident from IS and ^{27}Al MAS NMR results that a complete incorporation of aluminium in the matrix of Si-MCM-41 is necessary to obtain sufficiently high proton conductivities. Since sodium aluminate was found to be the best aluminium source for the preparation of samples exhibiting high proton conductivity we focused on the improvement of materials synthesized according this route by increasing the Al content, but still keeping a highly ordered mesoporous structure. Thus, we prepared samples with lower Si/Al ratio and thus more aluminium incorporated in the walls. Fig. 8 shows the powder XRD patterns for different $NaAlO_2$-MCM-41(y) samples with y varying in the range of $20 \geq y \geq 5$. It can be seen that the intensity of the (1 0 0) reflection decreases and broadens with increasing Al content. Besides the decreased reflection the loss of the long-range order can be denoted since even the (1 1 0) and (2 0 0) reflections disappear for $y \leq 10$. For the sample $NaAlO_2$-MCM-41(5) it finally disappears, indicating that a too high Al content in the walls weakens the order because with increasing number of negatively charged Al center ($[AlO_2]^{-1}$) in the framework their repulsive interactions and consequently the possibility to create point defects increase. The destruction of the Al-MCM-41 structure is confirmed in nitrogen adsorption measurements, documenting a decrease in pore volume and BET surface area (Table 1), for $NaAlO_2$-MCM-41(5). The strong collapse in surface area and especially in pore volume document the loss of mesoporosity.

Proton conductivities of $NaAlO_2$-MCM-41(y) samples with high aluminium content (Si/Al ratio down to 8) and still intact mesoporous structure were measured in IS at 100% relative humidity (Fig. 9). Again, compared to the pure silica based Si-MCM-41, the incorporation of tetrahedrally coordinated aluminium clearly increases the proton conductivity of all five samples in the entire temperature range. $NaAlO_2$-MCM-41(10) shows very high proton conductivities of up to 3×10^{-3} S cm^{-1} at 140 °C, being more than three orders of magnitude higher than in pure Si-MCM-41 in the whole measured temperature range. By incorporating few aluminium in the mesoporous SiO_2 framework and reaching a maximum ratio of Si/Al = 40, only a slight increase in proton conductivity compared to the pristine materials can be obtained. These aluminium silicates exhibit good mesoporous structure (Fig. 8). However, the distance between the fixed Brønsted acid sites in the framework is too large and several water molecules are necessary to bridge the proton transfer [8a]. Further increase of the

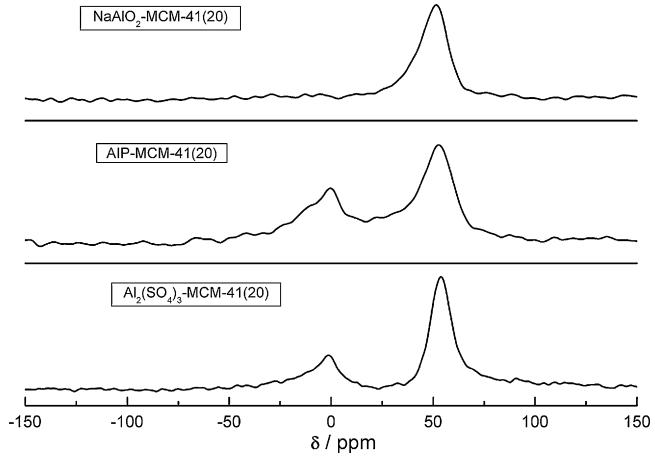

Fig. 7. ^{27}Al MAS NMR spectra of Al-MCM-41(20) samples synthesized with different Al sources.

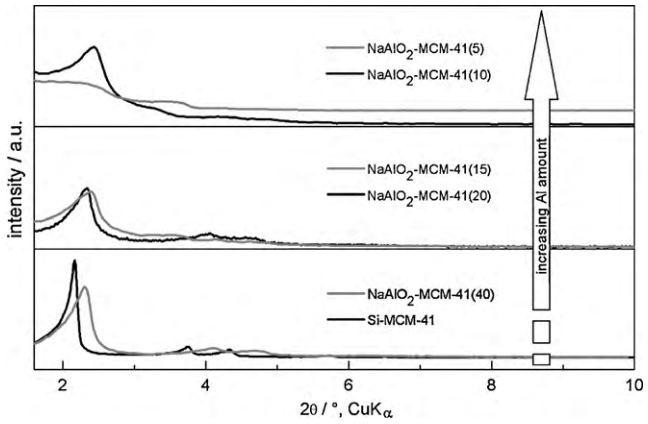

Fig. 8. XRD patterns of Si-MCM-41 and $NaAlO_2$-MCM-41 of different Si/Al ratio.

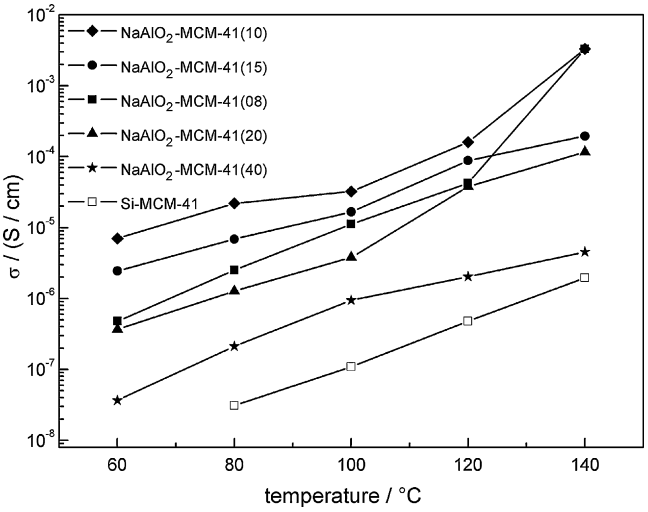

Fig. 9. Proton conductivities for Si-MCM-41 and $NaAlO_2$-MCM-41(y) of different Si/Al ratio at 100% RH. The lines are only to guide the eyes and have no physical meaning.

aluminium amount ($NaAlO_2$-MCM-41(y) with $20 \geq y \geq 10$) assures a sufficiently short distance of Brønsted acid sites for enhanced proton conductivity as shown by the sharp increase for $NaAlO_2$-MCM-41(20) in Fig. 9. Here the proton conductivity increases continuously up to a Si/Al ratio of 10. Although $NaAlO_2$-MCM-41(8) exhibits the highest aluminium amount its proton conductivity at 60–120 °C is worse than that of the samples $NaAlO_2$-MCM-41(10) and $NaAlO_2$-MCM-41(15) because the mesoporous structure is already damaged as seen from the decreased pore volume (Table 1) and the XRD pattern in Fig. 8. Therefore, the proton conductivity of the mesoporous material MCM-41 can only be improved continuously with increased aluminium content if the quality of the mesoporous hexagonal structure is sufficiently good for the proton transport inside the pores.

However, the proton conductivity of $NaAlO_2$-MCM-41(8) increases drastically for temperatures above 120 °C (Fig. 9). This effect can be ascribed to the higher hydrophilicity of that sample, helping to store more water in the pore system. Furthermore, only at increased temperatures the additional energy barriers in $NaAlO_2$-MCM-41(8) for the proton transport compared to those in $NaAlO_2$-MCM-41($y \geq 10$) samples caused by the decreased mesoporous hexagonal structure can be overcome due to the higher proton energy and an enhanced diffusion speed in the more water-rich environment.

4. Conclusions

Mesoporous Al-MCM-41 samples were synthesized by three different routes mainly varying the Al sources, and were compared to pristine Si-MCM-41 in proton conductivity and water storage. All Al-MCM-41 materials exhibit enhanced properties in both proton conductivity and water storage providing a stable and ordered mesoporous structure. The Al source $NaAlO_2$ gives clearly the best results, because all Al within the framework is tetrahedrally coordinated creating Brønstedt acidic centers. With $Al_2(SO_4)_3$ and AIP, however, also the presence of octahedral Al, which does not enhance the Brønstedt acidity of the framework, was observed. The enhancement of the proton conductivities results from improved water storage capabilities, decreased particle size from the micrometer to the nanometer scale (50–100 nm) and the creating Brønstedt acidity. The highest amount of incorporated Al in a mesoporous framework was obtained for the sample $NaAlO_2$-MCM-41(8). However, since the quality of the mesoporous material was slightly reduced distinct due to the high amount of aluminium incorporated, it does not show highest proton conductivity among the samples studied. The best proton conductivities were found for samples with Si/Al ratio of 10 where Al content and quality of the mesoporous structure are in optimum balance. These samples show conductivities of about 3×10^{-3} S cm^{-1} at 140 °C.

Acknowledgements

The work was supported by the Deutsche Forschungsgemeinschaft (DFG) (WA 1116/15, SPP1181) and the DAAD (D/07/01324). The authors thank Dr. Michaela Wilhelm (Ceramic Materials und Components, University of Bremen, Germany) for measuring water sorption isotherms, Dr. Jiří Rathouský (Heyrovský Institute of Physical Chemistry, Prague, Czech Republic) for measuring nitrogen isotherms, Prof. Paul Heitjans (Institute of Physical Chemistry, Leibniz University Hannover) for allowing us to use his NMR laboratory, and Prof. Jürgen Caro (Institute of Physical Chemistry, Leibniz University Hannover) for his fruitful contributions.

References

[1] P.P. Edwards, V.L. Kuznetsov, W.I.F. David, Phys. Eng. Sci. 365 (2007) 1043.
[2] B. Árnason, Int. J. Hydrogen Energy 25 (2000) 389.
[3] P.C. Ghosh, B. Emonts, H. Janßen, J. Mergel, D. Stolten, Solar Energy 75 (2003) 469.
[4] R. Marschall, I. Bannat, J. Caro, M. Wark, Micropor. Mesopor. Mater. 99 (2007) 190.
[5] R. Marschall, J. Rathousky, M. Wark, Chem. Mater. 19 (2007) 6401.
[6] J. Zhang, Z. Xie, J. Zhang, Y. Tang, C. Song, T. Navessin, Z. Shi, D. Song, H. Wang, D.P. Wilkonson, Z.-S. Liu, S. Holdcroft, J. Power Sources 160 (2006) 872.
[7] G. Alberti, R. Narducci, M. Sganappa, J. Power Sources 178 (2008) 575.
[8] (a) M. Wilhelm, M. Jeske, R. Marschall, W. Cavalcanti, P. Tölle, C. Köhler, D. Koch, T. Frauenheim, G. Grathwohl, J. Caro, M. Wark, J. Membr. Sci. 316 (2008) 164; (b) D. Gomes, R. Marschall, S.P. Nunes, M. Wark, J. Membr. Sci. 322 (2008) 406.
[9] R. Scheffler, A. Huth, G. Huebner, R. Marschall, J. Caro, M. Wark, Chem. Ing. Technol. 79 (2007) 2035.
[10] M.E. Franke, U. Simon, Solid State Ion. 118 (1999) 311.
[11] M.E. Franke, U. Simon, Chem. Phys. Chem. 5 (2004) 465.
[12] L. Rodriguez-Gonzales, F. Hermes, M. Bertmer, E. Rodriguez-Castellon, A. Jimenez-Lopez, U. Simon, Appl. Catal. A 328 (2007) 174.
[13] M.M.L. Ribeiro Carrott, F.L. Conceicao, J.M. Lopes, Micropor. Mesopor. Mater. 92 (2006) 270.
[14] R. Schmidt, Stud. Surf. Sci. Catal. 84 (1994) 61.
[15] E.P. Barrett, L.G. Joyner, P.P. Halenda, J. Am. Chem. Soc. 73 (1951) 373.
[16] R. Marschall, M. Sharifi, M. Wark, Micropor. Mesopor. Mater. 123 (2009) 21.
[17] S. Hitz, R. Prins, J. Catal. 168 (1997) 194.
[18] J.S. Beck, J.C. Vartuli, W.J. Roth, M.E. Leonowicz, C.T. Kresge, K.D. Schmidt, C.T.W. Chu, J. Am. Chem. Soc. 114 (1992) 10843.
[19] P.A. Russo, M.M.L. Ribeiro Carrott, Micropor. Mesopor. Mater. 103 (2007) 354.
[20] A. Matsumoto, H. Chen, K. Tsutsumi, Micropor. Mesopor. Mater. 32 (1999) 55.
[21] R. Mokaya, Catal. Lett. 37 (1996) 1891.
[22] M. Kruk, M. Jaroniec, Chem. Mater. 15 (2003) 2942.
[23] S.R. Zhai, C.S. He, D. Wu, Y.S.H. Sun, J. Non-Cryst. Solids 353 (2007) 1606.
[24] R. Mokaya, W. Jones, Z. Luan, M.D. Alba, J. Klinowski, Catal. Lett. 37 (1996) 113.
[25] S.-K. Song, Y. Wang, S.-K. Ihm, Catal. Today 111 (2006) 194.
[26] Zawodzinski Jr., A. Thomas, C. Derouin, S. Radzinski, J. Sherman, V.T. Smith, J. Electrochem. Soc. 140 (1993) 189.
[27] P. Costamagna, P. Srinivasan, J. Power Sources 102 (2001) 253.
[28] R. Marschall, I. Bannat, A. Feldhoff, L. Wang, G.Q. (Max) Lu, M. Wark, Small 5 (2009) 854.
[29] N. Eng-Poh, N. Hadi, W. Ka-Lun, Mohd Nazlan Mohd Muhid, H. Hamdan, Appl. Catal. A: Gen. 323 (2007) 58.